*Sensors and Materials*, Vol. 15, No. 5 (2003) 269–281
MYU Tokyo

S & M 0528

# Crystalline Si-Based Tunable Fabry-Perot Filter for In-Plane Optical Integration

Sung-Sik Yun and Jong-Hyun Lee

Department of Mechatronics, K-JIST
1 Oryong-Dong, Bukgu, Gwangju, 500-712, Korea

(Received March 26, 2003; accepted August 18, 2003)

***Key words:*** crystalline silicon, MEMS, tunable Fabry-Perot filter, silicon DRIE, in-plane, optical integration

In this paper, we present the crystalline Si-based tunable Fabry-Perot filter, which is able to be integrated for alignment with other optical devices on an in-plane substrate. The tunable Fabry-Perot filter is comprised of an air-gap resonator formed between two crystalline Si-reflecting mirrors fabricated by a silicon deep reactive ion etching (Si DRIE) process. The optical fibers can be horizontally aligned on the fabricated Fabry-Perot filter by exploiting an in-plane device structure. Tunability of the filter is achieved by changing the air-gap by actuating an electrostatic comb driver. The fabricated tunable Fabry-Perot filter showed high performance of the reflectance characteristics, such as a wide tuning range of over 80 nm and a high tuning sensitivity of 11.7 nm/V. When input voltage increases, a notch in the reflectance spectrum shifts to a longer wavelength and the wavelength tuning efficiency is 0.2 with respect to the displacement of a movable reflecting mirror. The response time for wavelength tuning was demonstrated to be less than 5 ms for both up and down tuning of 45 nm.

## 1. Introduction

Tunable Fabry-Perot filters are key components for implementing a spectroscopy or wavelength-division-multiplexing (WDM) network.[1–4] Moreover, owing to its high sensitivity to changes of cavity length, the Fabry-Perot interferometer has been widely used to measure the displacement with nanometer resolution.[5] Recently, micromachining technologies have been introduced as a new approach to the fabrication of the tunable

*Corresponding author, e-mail address: jonghyun@kjist.ac.kr

Fabry-Perot filters using two vertically distributed Bragg reflectors.[6–9] These micromachined tunable Fabry-Perot filters have the merits of low insertion loss, wide tuning range and small size. However, fabrication of the previous Fabry-Perot filters required a multiple deposition process on a substrate because several dielectric optical layers should be stacked up to build distributed Bragg reflectors for obtaining a high reflection. Packaging these vertical Fabry-Perot filters and their connection with other optical components are also complicated because the multilayered Fabry-Perot filters require a vertical fiber alignment onto the substrate.

In this paper, we present a crystalline Si-based tunable Fabry-Perot filter that is horizontally located for in-plane optical integration. The proposed tunable filter is comprised of a Fabry-Perot resonator with the air-gap formed between two crystalline Si-reflecting mirrors. An electrostatic comb actuator mechanically modulates the air-gap of the resonator to tune the central wavelength in a reflection band. The entire in-plane device is fabricated using the Si DRIE process of a silicon-on-insulator (SOI) wafer. Optical fibers can be easily aligned along with a tunable Fabry-Perot filter by the proposed in-plane filter structure, which also enables the tunable Fabry-Perot filters to be easily connected to other optical components. By employing the crystalline silicon, we can also alleviate the potential problems of uncertain material properties, stress-induced deformation and non-uniform gap control that frequently degrade the performance of the vertically stacked Fabry-Perot filter.

## 2. Tunability Design

### 2.1 *Design principles*

The principle of the proposed tunable optical filter is based on a Fabry-Perot interferometer, as shown in Fig. 1. The tunable Fabry-Perot filter employs an optical resonator with an air-gap and two partially reflecting mirrors made of crystalline silicon. The air-gap predominantly determines the central wavelength and even a single silicon layer shows sufficiently large reflectance due to its high refractive index ($n_r$=3.479). The layer thickness of the air resonator and two reflecting mirrors should be equal to the integer

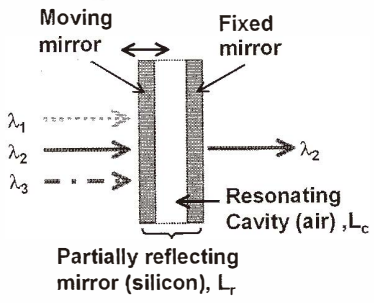


Fig. 1. Schematic of the micromachined in-plane Fabry-Perot filter with an air-gap resonator and two partially reflecting mirrors.

multiple of $\lambda_c/2$ and $\lambda_c/4$, respectively, where $\lambda_c$ is the central wavelength of the reflectance spectrum. Equations (1a) and (1b) represent the required thickness of each dielectric layer of the proposed Fabry-Perot filter;

$$L_r = \left(\frac{1}{2}N_r + \frac{1}{4}\right)\frac{\lambda_c}{n_r}, \tag{1a}$$

$$L_c = \left(\frac{N_c}{2}\right)\frac{\lambda_c}{n_c}, \tag{1b}$$

where $L_r$ and $L_c$ are the designed thicknesses of the partially reflecting Si mirror and the air-gap of the optical resonator, respectively. $n_r$ and $n_c$ are the refractive indices of the partially reflecting Si mirror and the air-gap of the resonator, respectively. $N_r$ and $N_c$ are integer numbers related to the actual thickness of each layer, and the integer numbers are determined to have the smallest feasible value considering a critical linewidth in the fabrication process.

In order to implement a steeper Fabry-Perot filter, we can employ two distributed Bragg reflectors with several layers of silicon plates. The larger counts of silicon plates in each Bragg reflector show a higher reflectance, which leads to a narrow reflection or transmission band at the central wavelength.[9] The large difference in the refractive index between the Si layer and air-gap also induces a high reflectance in the DBR, which is one of the reasons why we selected crystalline silicon as a partially reflecting layer. Another reason for the selection of silicon is that the property of crystalline silicon is known to be sufficiently stable for the fabrication and reliable operation of optical devices.

## 2.2 *Tuning mechanism*

The proposed optical filter employs the modulation of the air-gap optical resonator for tunability, and is comprised of a Fabry-Perot interferometer and two crystalline Si-reflecting mirrors, as shown in Fig. 2. When light propagates normally in the optical filter,

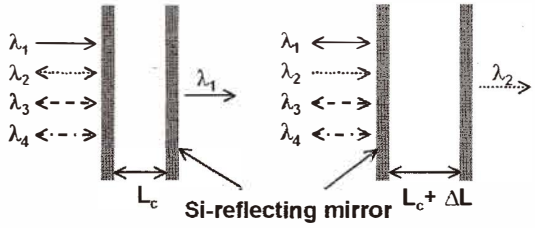


Fig. 2. Schematic diagram of tuning mechanism in the proposed tunable Fabry-Perot filter; (a) initial state, (b) up-tuning state.

multibeam interference occurs in each dielectric layer of the air-gap resonator and in the crystalline Si-reflecting mirrors. This interference in the air-gap resonator determines the wavelength spectrum of the Fabry-Perot filter, which can be calculated by the overall transfer matrix, the product of the individual transfer matrices.[10] The reflection coefficient ($r$) can be expressed by eq. (2), then the reflectance, $R$, is given by $R = |r|^2$.

$$r = \frac{An_0 + Bn_T n_0 - C - Dn_T}{An_0 + Bn_T n_0 + C + Dn_T}, \tag{2}$$

where $n_0$ and $n_T$ are refraction indices of air and silicon, and $A$, $B$, $C$, $D$ are the elements of the overall transfer matrix.

Figure 3 shows the theoretical reflectance spectrum of the proposed tunable Fabry-Perot filter calculated by the transfer matrix and the estimated displacement of the air-gap with respect to the selected wavelength. The center wavelength of the designed Fabry-Perot filter is 1550 nm and the available range of tuning wavelength is from 1520 nm to 1580 nm. The tuning efficiency is defined by the ratio of tuned wavelength and cavity change, and is given by eq. (3);

$$\frac{\Delta\lambda}{\Delta L} = \frac{\lambda_0}{L_{eff}}, \tag{3}$$

where $\Delta\lambda$, $\Delta L$, $\lambda_0$, and $L_{eff}$ are the tuning range, the cavity change, wavelengths of notches and effective cavity length, respectively.[8,11] The tuning shows a linear characteristic in the wavelength range of 60 nm corresponding to the cavity change of 300 nm, and the tuning efficiency is 0.2 for the designed filter.

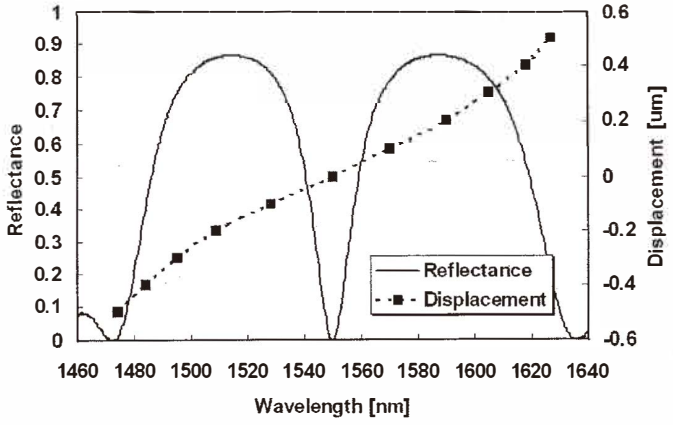


Fig. 3. The calculated reflectance spectrum of the proposed tunable Fabry-Perot filter and the estimated displacement of the air-gap with respect to each selected wavelength.

## 3. Materials and Fabrication Methods

The structure of the proposed Fabry Perot filter consists of the optical plates fabricated on the SOI wafer and the fixed optical fiber in an air-ambience, as shown in Figs. 4(a) and (b). The tunable Fabry-Perot filter is located horizontally, and the optical fiber is aligned on the SOI substrate in order to experimentally investigate the reflectance characteristics. The in-plane fiber assembly was so simple that we could complete the assembly sequence solely by laying a fiber into the U-shaped groove and by UV-glue bonding with no active alignment. The proposed Fabry-Perot filter can also take advantage of easy connection with other optical components by exploiting the in-plane device structure.

The proposed Fabry-Perot filter was simply fabricated by the anisotropy Si DRIE process of SOI wafer with a structural Si layer of 80 $\mu$m thickness and a sacrificial oxide layer of 2 $\mu$m thickness. The SOI wafer is fabricated by fusion bonding of two wafers, the device wafer and the handle wafer with an intermediate thermally oxidized 2-$\mu$m-thick $SiO_2$ layer. The resistivity of the device wafer is as small as 0.01 $\Omega$cm so that additional doping is not necessary for obtaining a conductive layer (Fig. 5(a)). The actual fabrication process starts with the deposition of oxide film of 1 $\mu$m thickness by a plasma-enhanced chemical vapor deposition (PECVD) process. The spin-coated photoresist on the oxide was patterned by standard photolithography (Fig. 5(b)). Then, the oxide was patterned by dry etching to form an etch mask of Si DRIE, and then the photoresist was stripped (Fig. 5(c)).

The Si device layer of the SOI wafer was then vertically etched using the DRIE process (Fig. 5(d)). The DRIE process made use of a fluorine-based chemistry that allows high aspect ratio etches using alternating etch and sidewall passivation steps. Inductively coupled plasma (ICP) is utilized to provide high-density plasma in the Si DRIE process. In order to free the movable structures, the reflecting mirrors and comb actuator were released by etching the buried sacrificial oxide with anhydrous gas-phase hydrogen fluoride (HF) (Fig. 5(e)).[12] The PECVD oxide etch mask is simultaneously removed with sacrificial oxide.

Finally, an optical fiber coated with an antireflection (AR) coating was aligned in the U-groove micromachined during the Si DRIE process, in order to optically characterize the

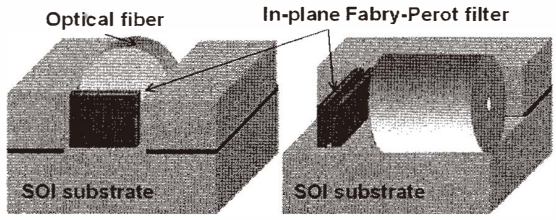


Fig. 4. Cross-sectional view of the proposed in-plane tunable Fabry-Perot filter fabricated on the SOI wafer: (a) front view and (b) side view.

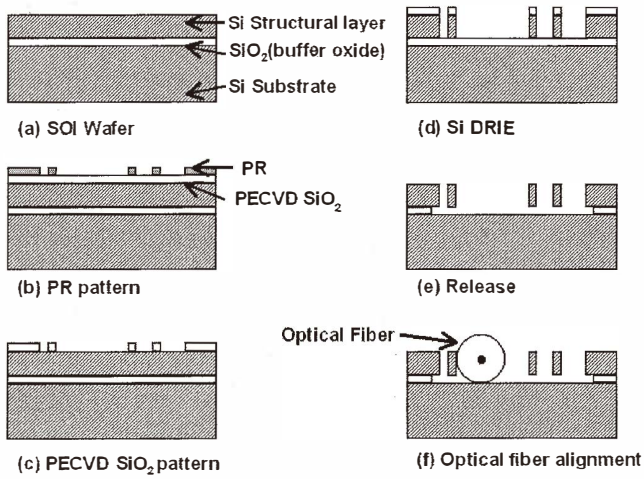


Fig. 5. Fabrication sequence of a micromachined in-plane tunable Fabry-Perot filter; (a) a SOI wafer, (b) PR pattern, (c) a PECVD oxide mask pattern, (d) a Si DRIE, (e) PECVD oxide removal and sacrificial oxide etching and (f) passive alignment of optical fibers.

fabricated in-plane Fabry-Perot filter (Fig. 5(f)). Note that the entire fabricated device was horizontally located, and the optical fiber was horizontally aligned with the Fabry-Perot filter structure on the substrate to exploit the easy alignment of the optical fiber. Figure 6 shows the overall scanning electron microscope (SEM) image of the fabricated in-plane tunable filter. The filter structure and U-groove have an 80 $\mu$m height in order to satisfy the required area for an optical window for sufficient multiple interference in the Fabry-Perot filter.

## 4. Experimental Results and Discussion

### 4.1 *Experimental setup*

Figure 7(a) illustrates the schematic of the experimental setup for measuring the performance of the fabricated in-plane Fabry-Perot filter. To evaluate the tunability of the filter, the light emitted from an amplified spontaneous emission (ASE) broadband source propagates onto the in-plane Fabry-Perot filter through optical fibers and an optical spectrum analyzer (OSA) detects the reflection spectrum from the fabricated Fabry-Perot filter. The ASE broadband source has a peak wavelength of 1550 nm and a 3 dB bandwidth of 52 nm. The optical circulator redirects the reflected light from the filter under test to the optical power meter. Figure 7(b) shows a photograph of the actual experimental setup and the detailed optical alignment apparatus.

The optical fibers were passively aligned into the fabricated U-groove using the 6-axis precision fiber aligner monitoring a status of fiber alignment with a CCD camera, as shown in Fig. 7(b). In the preparation of the optical fibers, the flat-ended fiber with no AR coating might cause an undesirable effect due to multibeam interference between the fiber and the

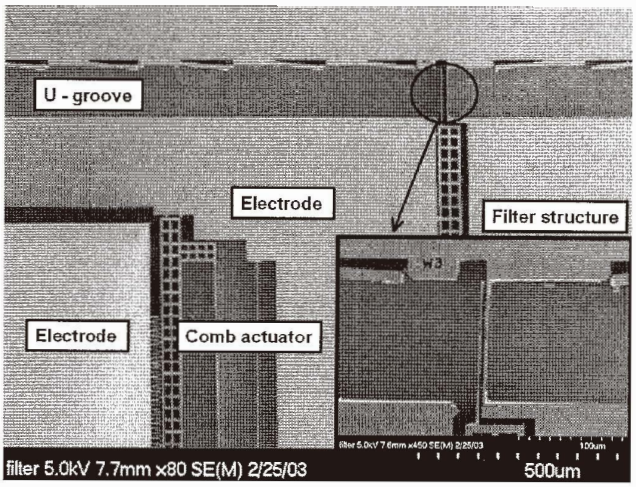


Fig. 6. SEM images of overall view and detailed view of the fabricated in-plane Fabry-Perot filter.

(a)

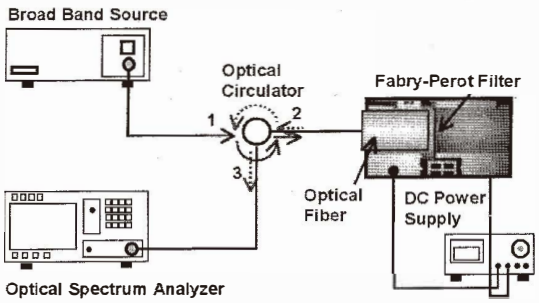


(b)

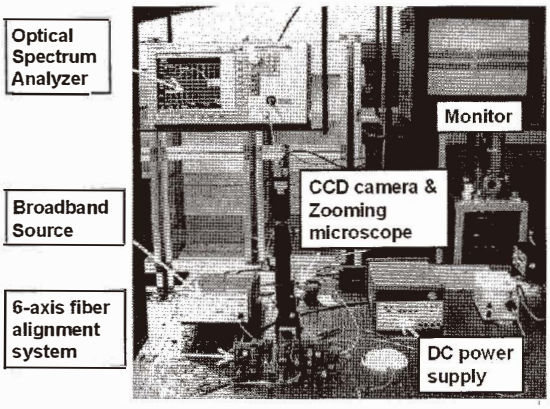


Fig. 7. The experimental setup for measuring optical performances of the Fabry-Perot filter: (a) schematic, (b) photograph of the overall view.

Fabry-Perot filter, and distortion in the spectral response of the filter. Hence, the optical fibers were coated with an AR coating, which reveals a back reflection under –30 dB for 1500 nm to 1600 nm. The wavelength tuning is achieved by varying the air-gap between two reflecting mirrors using the electrostatic comb actuator in an ambient condition.

### 4.2 *Actuation characteristics*

Fabricated tunable Fabry-Perot filters were experimentally evaluated regarding their electromechanical actuation characteristics. For measuring the displacement, input sinusoidal voltage was applied to the electrostatic comb actuator. The driving frequency was 100 Hz, which is sufficiently high to obtain a good signal from the in-plane laser vibrometer and is also far below the resonant frequency of the comb actuator. Figure 8 compares the experimental displacement with two theoretical values for the electrostatic comb actuator. The designed and estimated value for theoretical displacement is calculated using an initial dimension in the mask layout and the actual dimension of the fabricated device measured by SEM, respectively.

Actually the measured width of the spring was 2.6 $\mu$m, which is a little larger than the designed value of 2.4 $\mu$m. The difference between these two values is believed to result in a discrepancy of 20% in Fig. 8 since the width of the spring dominates the displacement of the comb actuator. The output of the laser vibrometer tends to depend upon the surface roughness and shows around 10% variation for different measuring points of the same sample. The measurement error of the vibrometer can explain why the estimated displacement still has a mismatch by 10% compared with the experimental one.

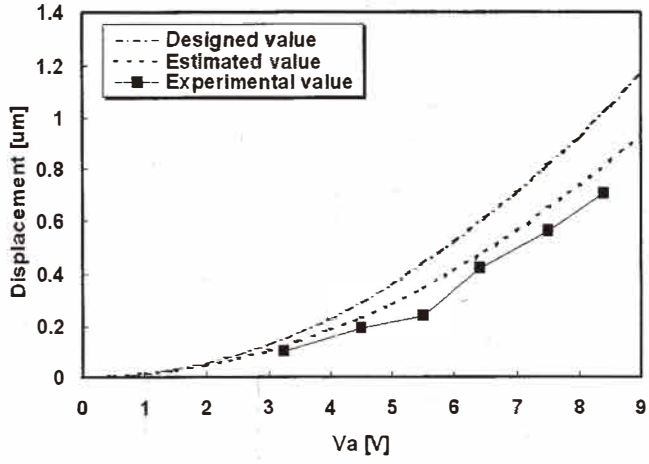


Fig. 8. The theoretical and experimental characterization of the displacement of the electrostatic comb actuator for the fabricated tunable Fabry-Perot filter.

### 4.3 *Optical characteristics*

We investigated the reflectance characteristics of the fabricated in-plane tunable Fabry-Perot filter. Figure 9 shows an experimental reflectance curve with respect to input voltage. The experimental initial wavelength of the notch in the reflectance spectrum was 1534 nm, although the designed initial wavelength was 1550 nm. This is because the actual air-gap between the two reflecting mirrors is narrower than the designed one due to the microloading effect in the Si DRIE process. As the input voltage increases, the reflectance curve shifts to a longer wavelength with a sensitivity of 11.7 nm/V. The total insertion loss is less than 5 dB, including a scattering loss of the reflecting mirrors, a coupling loss of the fibers, an insertion loss of an optical circulator and connecting losses between patch codes.

Figure 10 shows the shift of notch wavelength and its FWHM (Full Width at Half Maximum) according to the variation of applied voltages to the fabricated tunable Fabry-

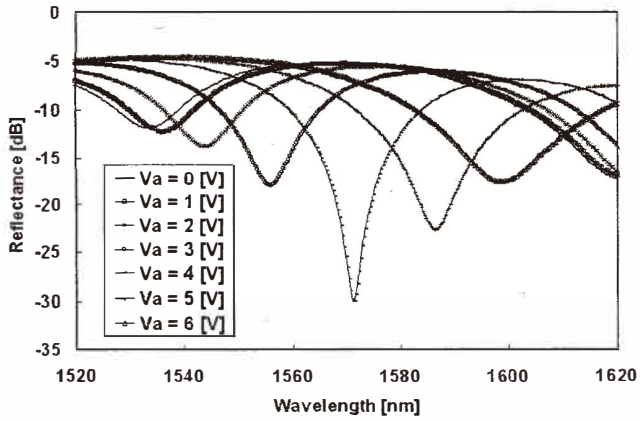


Fig. 9. Measured reflectance spectrum of the micromachined in-plane Si optical filter.

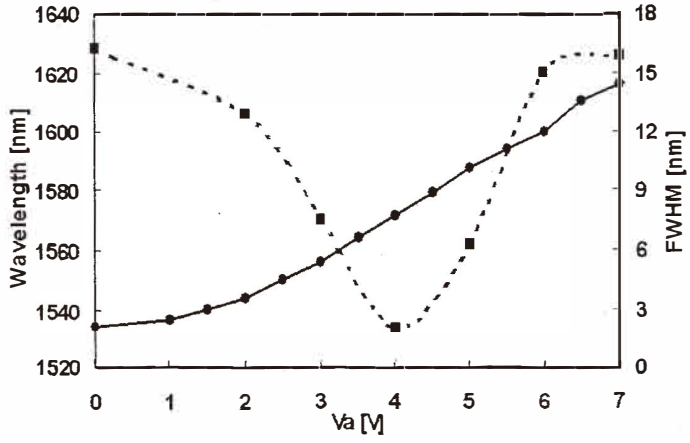


Fig. 10. Measured wavelength tuning and FWHM of the reflectance spectrum with respect to applied voltages for the fabricated tunable Fabry-Perot filter.

Perot filter. The FWHM is usually defined as 3 dB above the minimum notch value because this is useful in a realistic reflective optical filter.[6] The FWHM of the notch was as small as 2.1 nm at the wavelength of 1570 nm, and increased to 16 nm at the outskirts of the spectrum. The FWHM value can be improved by increasing the reflectance of reflecting mirrors by adding pairs of Si-air Bragg reflecting mirrors, which could be theoretically confirmed by the simulation using a transfer matrix.[10]

Figure 11 shows selected wavelengths with respect to the displacements of the partially reflecting mirror. The estimated tuning wavelength is in good agreement with the experimental ones, but considerable discrepancy was found between the designed and estimated ones due to the fabrication error. The linear tuning range was about 37 nm corresponding to the actuator displacement of 180 nm. The tuning efficiency is calculated to be 0.2 in the linear tuning range and effective cavity length was estimated to be 7.67 $\mu$m at the wavelength of 1534 nm from eq. (3).

When the notch wavelength in the reflectance spectrum approaches either end of the stop band, the tuning efficiency decreases because the reflectivity of the Si partial mirrors decreases less near both sides of the stop band. The mismatch between estimated and experimental values at a large displacement over 0.5 $\mu$m could be explained by the fact that the bandwidth of the ASE broadband source is available at the wavelength below 1600 nm.

In the fabrication of the vertical sidewalls, the DRIE process might frequently come with considerable surface roughness and verticality error. The roughness and verticality error of the fabricated Fabry-Perot filter were experimentally achieved to be 20 nm (rms) and 0.2 degree (for the effective area of 20×20 $\mu$m$^2$ of silicon plates), respectively. Based on the imperfection analysis, it was confirmed that the roughness and verticality degrade the finesse of the cavity by 10% and 32%, respectively.[13] The finesse is defined as the ratio of tuning range (FSR) over FWHM, which is one of the important performance indices in the evaluation of the fabricated Fabry-Perot filter.

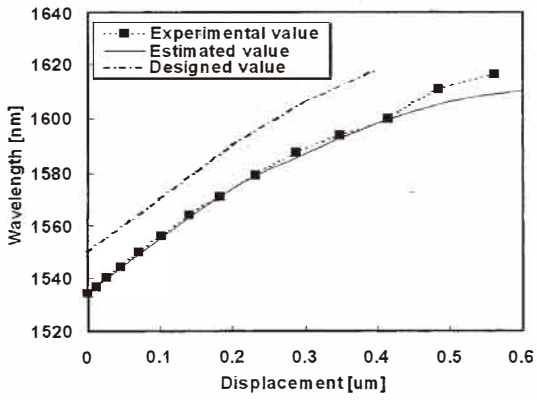


Fig. 11. Wavelength tuning by the change in the air-gap of the optical resonator. The designed, estimated and experimental values are compared with respect to the displacement of the partially reflecting mirror.

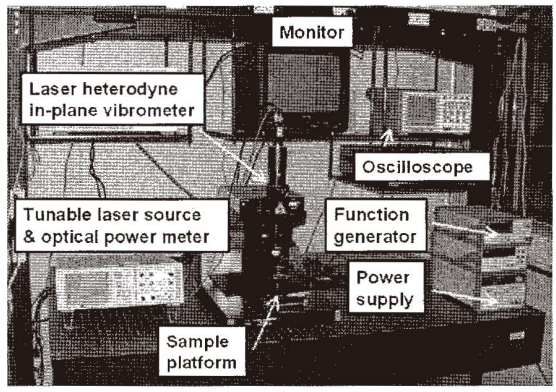


Fig. 12. Experimental setup comprising laser vibrometer, tunable laser source, and optical power meter for measuring dynamic and optical characteristics of the in-plane tunable Fabry-Perot filter.

### 4.4 *Experimental response time*

We measured dynamic characteristics of the mechanical and optical output for the fabricated in-plane tunable Fabry-Perot filter. Figure 12 shows the experimental setup for measuring the dynamic response and optical tuning response of the tunable Fabry-Perot filter using a laser heterodyne in-plane vibrometer, tunable laser source, function generator, oscilloscope and optical power meter.

We measured both cases of time responses, tuning up and tuning down. The wavelength is tuned from 1534 nm to 1579.5 nm when applied voltage changes from 0 V to 4.5 V. The other case of tuning-down can be obtained by a reverse operation. For the measurement of optical time response, a tunable laser source was used at a constant 1581.5 nm with optical power of 1 mW. The operating wavelength was selected to obtain large fluctuation of optical output by taking advantage of the large slope in the reflectance spectrum, as shown in Fig. 13(a). The dynamic response of the movable Si partial mirror was illustrated with optical output in Fig. 13(b) in the case of tuning up. The change of optical power (A) and the displacement of microactuator (B) are 15.65 dB and 180 nm, respectively, which agree well with the values in Fig. 13(b). The overshoot of the electrostatic comb actuator brought about two abnormal oscillations in the optical time response, due to the fact that the tuned wavelength showed ringing over the notch wavelength of 1579 nm at the applied voltage of 4.5 V. The settling times of both the optical and mechanical responses were measured to be less than 5 ms.

In the case of tuning down, the notch wavelength in the reflectance spectrum returns to 1534 nm. We did not notice any abnormal oscillations in the optical response because the slope of the reflectance curve is small at the operating wavelength of 1581.5 nm. The settling time of the optical response for tuning down was reduced to 2 ms, even though the settling time of the mechanical response was still 5 ms. The settling time of tuning up can be improved by considering a squeeze damping in the dynamic design and the resonant frequency was estimated to be around 1.2 kHz from the ringing frequency.

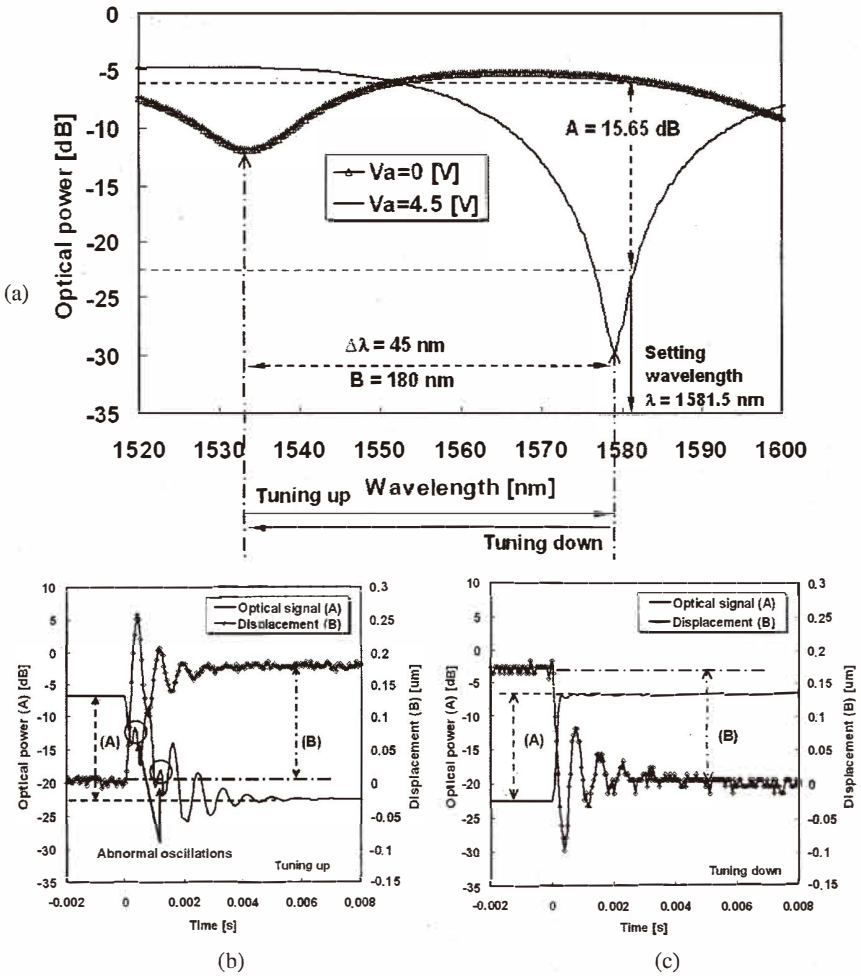


Fig. 13. Dynamic responses of optical signal and displacement for the fabricated tunable Fabry-Perot filter; (a) two reflectance curves used for wavelength tuning up and tuning down, (b) wavelength tuning up, (c) wavelength tuning down.

## 5. Conclusions

We have designed and fabricated a crystalline Si-based Fabry-Perot filter for in-plane optical integration. The proposed optical filter employs the modulation of the gap between two Si plates for tunability, and is comprised of a Fabry-Perot air resonator and two crystalline Si reflecting mirrors. The entire device was horizontally fabricated using the Si DRIE process on SOI wafers for in-plane alignment with other optical components.

Tunability of the Fabry-Perot filters was achieved through air-gap modulation by an electrostatic comb actuator. As input voltage increases, the notch level of the reflectance spectrum shifts to a longer wavelength with a tuning range of over 80 nm and the sensitivity of 11.7 nm/V. The wavelength tuning efficiency is 0.206 with respect to the displacement between two reflecting mirrors. The settling time for wavelength tuning was within 5 ms for a step voltage signal of 4.5 V. In conclusion, the proposed in-plane tunable filter was confirmed to feature a wide tuning range, easy alignment of optical fibers and simple connection with other optical components using in-plane optical integration.

## Acknowledgements

The authors would like to thank Mr. Kyungwoo Jo, K-JIST, for technical discussion. This research was supported by a grant (code # FN02-0302-001-1-0-1) from the Center for Nanoscale Mechatronics & Manufacturing of the 21st Century Frontier Research Program.

## References

1 G. Lammel, S. Schweizer and P. Renaud: The 14th IEEE International Conference on MEMS (2001) p. 578.
2 D. Sadot and E. Boimovich: IEEE Communications Magazine **36** (1998) 50.
3 G. Cocorullo, F.G. Della Corte, M. Iodice and I. Rendina: Digest of the LEOS Summer Topical Meetings (2000) p. 45.
4 S. S Yun and J. H Lee: Proceedings of SPIE vol. 4983 (2003) p.195.
5 B. Chen, R. Zhu, Z. Wu, D. Li and S. Guo: Applied Optics **40** (2001) 5632.
6 D. Hohlfeld, M. Epmeier and H. Zappe: The 15th IEEE International Conference on MEMS (2002) p. 564.
7 C. F. R. Mateus, C. H. Chang, L. Chrostowski, S. Yang, D. Sun, R. Pathak and C. J. Chang-Hasnain: IEEE Photonics Technology Letters **14** (2002) 819.
8 R. LeDantec, T. Benyattou, G. Gillot, A. Spisser, C. Seassal, J. L. Leclercq, P. Viktorovitch, D. Rondi and R. Blondeau: IEEE Journal of Selected Topics in Quantum Electronics **5** (1999) 111.
9 H. Hillmer, J. Daleiden, C. Prott, F. Romer, A. Tarraf, S. Irmer and V. Rangelov: Proceeding of SPIE vol. 4646 (2002) p. 19.
10 G. R. Fowles: Introduction to Modern Optics, Dover ed., Chap. 4 (1989).
11 D. I. Babic and S. W. Corzine: IEEE Journal of Quantum Electron **28** (1992) 514 .
12 J. H. Lee, W. I. Jang, C. S. Lee, Y. I. Lee, C. A. Choi, J. T. Baek and H. J. Yoo: Sensors and Actuators A **64** (1998) 27.
13 P. D. Atherton, N. K. Reay, J. Ring and T. R. Hicks: Optical Engineering **20** (1981) 806.